



1 Complexity in Biogeochemical Models: Consequences for the Biological Carbon Pump

2

3 Jonathan Rogerson^{1*}, Alessandro Tagliabue², Agathe Nguyen¹, Marcello Vichi^{3,4}, Lewis Wrightson²,
4 Prima Anugerahanti^{2,5}, Olivier Aumont⁶ & Marion Gehlen¹

5

6 ¹Laboratoire des Sciences du Climat et de l'Environnement, LSCE/IPSL, CEA-CNRS-UVSQ, Université Paris-Saclay,
7 Gif-sur-Yvette, FR. ²Department of Earth Ocean, and Ecological Sciences, School of Environmental Sciences,
8 University of Liverpool, Liverpool, UK. ³Department of Oceanography, University of Cape Town, Cape Town, RSA.
9 ⁴Marine and Antarctic Research centre for the Innovation and Sustainability (MARIS), Cape Town, RSA. ⁵National
10 Oceanography Centre, Liverpool, UK. ⁶Sorbonne Université, CNRS/IRD/MNHN, LOCEAN-IPSL, Paris, FR.

11

12 *Corresponding author: Jonathan Rogerson: jonathan.rogerson@lsce.ipsl.fr

13

14 Abstract

15

16 Ocean biogeochemical models underpin projections of future marine ecosystem change, including
17 anticipated shifts in the biological carbon pump (BCP) and broader biogeochemical cycles.
18 However, their outputs remain highly sensitive to model complexity and parameterisation choices.
19 Here, we evaluate five configurations of the Pelagic Interaction Scheme for Carbon and Ecosystem
20 Studies (PISCES) to quantify intramodel variability in net primary productivity (NPP), carbon
21 export (C_{exp}), and export efficiency (e-ratio) over the 21st century under the high emissions RCP8.5
22 scenario. The tested PISCES configurations differed from the standard model through distinct
23 modifications to phytoplankton growth processes, but are forced by identical physical variables,
24 representing an ensemble opportunity. All configurations resolve NPP and C_{exp} within the range of
25 remote-sensing variability. The more complex Quota-based configurations produce 15-21 (10-18)
26 Pg C yr⁻¹ more NPP than the simpler Monod-quota models in the reference (future) period, but this
27 increase, driven by elevated small phytoplankton biomass, does not enhance C_{exp} , yielding lower
28 e-ratios (0.14-0.17) than in the Monod-quota configurations (~0.25). The introduction of a
29 picophytoplankton functional type (PFT) emerges as one of the most influential parameterisation
30 choices. It drives opposing future NPP responses between 30-60° N/S, an increase in the
31 Monod-quota configurations versus a decline in the Quota-based ones, as well as contrasting
32 latitudinal trends in C_{exp} within the same region. Other parameterisations, such as a low-iron
33 scheme, an added diazotroph PFT, and explicit manganese cycling, exert more modest, regionally
34 confined effects under high emissions scenarios, influencing NPP and C_{exp} primarily at biome scales
35 rather than driving large-scale divergence in model behaviour.

36

37 Plain language summary

38

39 We use five different versions of a biogeochemical model to show that how phytoplankton growth
40 processes are represented strongly shapes projections of future ocean productivity and carbon
41 export. Added model complexity does not have a uniform global effect as some new processes
42 mainly influence specific ocean regions, while others, such as an additional small phytoplankton
43 type, lead to large intramodel differences in future trends and latitudinal patterns of productivity and
44 carbon export.

45

46 Key words: biogeochemical modelling, parameterisations, biological carbon pump, export

47

48 1. Introduction

49

50 The biological carbon pump (BCP) plays a critical role in regulating Earth's climate by facilitating
51 the vertical transport of carbon from the surface to the deep ocean, thereby helping to remove
52 atmospheric CO₂ on centennial to millennial timescales (Falkowski et al., 1998, 2000; Buesseler et



53 al., 2007; Visser, 2025). Since pre-industrial times (~280 ppm), global atmospheric CO₂
54 concentrations have risen by 51%, reaching 419 ppm as of the present (Friedlingstein et al., 2023).
55 This increase has contributed to a ~1.5 °C rise in average global surface temperatures, with the
56 previous decade (2014-2024) marking the warmest on record (Ripple et al., 2024; WMO, 2025).
57 The ocean has absorbed 20-30% of anthropogenic CO₂ emissions since the mid-1980s (Sabine et
58 al., 2004; Bindoff et al., 2019), equivalent to 2.1–2.4 Pg C yr⁻¹ (DeVries et al., 2023). Stand-alone
59 ocean model studies suggest that, at equilibrium, BCP-mediated processes result in baseline
60 atmospheric CO₂ concentrations being 150-200 ppm lower than they would be otherwise in their
61 absence (Maier-Reimer et al., 1996; Falkowski et al., 2000). A fully interactive Earth System Model
62 (ESM) refines this estimate, showing a 163 ppm increase in pre-industrial CO₂ when marine
63 ecosystems are removed (Tjiputra et al., 2025). The BCP therefore represents a substantial
64 ecosystem service, valued at \$0.8-1.1 trillion per year globally (Berzaghi et al., 2025).
65 Understanding how the biological processes that underpin the BCP, and its efficiency, will respond
66 to climate change remains an important and active area of research (Jin et al., 2020).

67

68 Through air-sea gas exchange, atmospheric CO₂ dissolves into the surface ocean, increasing the
69 dissolved inorganic carbon (DIC) pool. In the ocean, this DIC is absorbed and sequestered through
70 two mechanisms, the solubility pump and BCP. The solubility pump is driven by the combination of
71 thermodynamic and physical processes that slowly transport DIC from the surface ocean into the
72 interior via mode and deep water formation. It is the dominant mechanism for the uptake and
73 transport of anthropogenic CO₂ from the surface ocean to below the mixed layer (Bindoff et al.,
74 2019). The BCP further facilitates this vertical transport of carbon through the export of particulate
75 organic carbon (POC), synthesised via phytoplankton net primary productivity (NPP) in the sunlit
76 surface ocean. The subsequent sinking and export (C_{exp}) of POC out of the euphotic zone and into
77 the deep ocean (> 1000 m) contributes to the long-term removal of carbon on timescales of
78 hundreds to thousands of years (Falkowski et al., 1998, 2000; Buesseler et al., 2007; Visser, 2025).
79 Phytoplankton photosynthesis lowers the partial pressure of CO₂ in the surface ocean while export
80 production sustains the vertical gradients in DIC necessary to promote the absorption of CO₂ from
81 the atmosphere. Therefore, the BCP emerges as a critical, climate-relevant pathway in the ocean's
82 role as a long-term carbon sink (Falkowski et al., 2000; Sigman and Boyle, 2000).

83

84 In the upper ocean, most of the produced POC is rapidly remineralised, with only a small fraction
85 (~20%) being exported below 100 m (Falkowski et al., 2000; Laws et al., 2000; Ducklow et al.,
86 2001; Henson et al., 2012; Siegel et al., 2014; Nowicki et al., 2022). The efficiency of the BCP,
87 commonly denoted as the e-ratio (= C_{exp}/NPP), principally determines how much fixed carbon is
88 exported from the surface ocean to depth, indirectly influencing the long-term sequestration of
89 atmospheric CO₂. A consensus emerging from multi-model intercomparison studies is that global
90 warming will lead to higher sea surface temperatures (SSTs), increased stratification, ocean
91 acidification, and reduced oxygen solubility by the end of the 21st century (Steinacher et al., 2010;
92 Bopp et al., 2013; Bindoff et al., 2019; Kwiatkowski et al., 2020). In response to these changing
93 physical environmental conditions, marine ecosystems (Frémont et al., 2022) and phytoplankton
94 community composition (Bopp et al., 2005; Basu and Mackey, 2018; Tréguer et al., 2018; Benedetti
95 et al., 2021; Henson et al., 2021; Fisher et al., 2025) are expected to be impacted, which will have
96 consequences for ocean productivity and export production.

97

98 Capturing the complexity of the BCP remains a major challenge in ESMs (Doney et al. 2024).
99 Across successive generations of Carbon Model Intercomparison Project(s) (CMIP), there is
100 substantial intermodel variability in projected 21st century NPP and C_{exp} (Bopp et al., 2013;
101 Laufkötter et al., 2015, 2016; Kwiatkowski et al., 2020; Tagliabue et al., 2021; Wilson et al., 2022),
102 reflecting large differences in how models represent key biogeochemical processes and marine



103 ecosystem complexity (Séférian et al., 2020; Henson et al., 2022). Under the high-emissions
104 scenario SSP5-8.5, CMIP6 models project export production to change by -41% to +1.8% relative
105 to the historical period (Henson et al., 2022) and relative to present-day conditions, global NPP is
106 projected to decline by 1.76%, with a model standard deviation of 8.06% (Tagliabue et al., 2021).
107 Furthermore, future declines in NPP are likely underestimated within the CMIP6 ensemble,
108 considering their contemporary trends relative to remote-sensing (Ryan-Keogh et al., 2025).

109

110 Within the CMIP ensemble, a wide range of biogeochemical models is represented (e.g. BEC –
111 Moore et al., 2001, 2004; BFM – Vichi et al., 2007; PISCES – Aumont et al., 2015; REcoM2 –
112 Hauck et al., 2013; TOPAZ – Dunne et al., 2012), each differing in its complexity and
113 parameterisation of key biogeochemical processes. Although model intercomparison projects have
114 provided valuable insights into the global BCP, it remains unclear how differences in these
115 biogeochemical parameterisations, and complexity thereof, contribute to the divergence among
116 CMIP models in their projections of the BCP over the 21st century. Most model intercomparison
117 studies evaluate different architectures against common criteria to identify model shortcomings and
118 ensemble-wide patterns (Fennel et al., 2022). However, pinpointing sources of divergence and the
119 role of individual parameterisations is challenging within this context. An alternative is to compare
120 different parameterisations within the same biogeochemical model under identical physical forcing,
121 enabling variability arising solely from biogeochemical differences to be isolated.

122

123 This study employs the PISCES ocean biogeochemical model (Aumont et al., 2015) in a suite of
124 distinct configurations under high emissions RCP8.5 scenario to isolate how differences in
125 biogeochemical parameterisations and complexity drive variability in the BCP over the 21st century.
126 The methodology details the various PISCES configurations and their nuances while the results are
127 presented in two parts. In the first, we compare present-day PISCES outputs with remote-sensing
128 data to evaluate whether variations in biogeochemical parameterisations and complexity lead to
129 discernible differences in NPP and export production at global and biome scales. The second
130 examines how these variables evolve between present/reference (1986–2005) and future
131 (2091–2100) projections, highlighting how differences in top-down processes propagate through
132 NPP and C_{exp} . Ultimately, the study identifies key biogeochemical parameterisations that strongly
133 shape ecosystem dynamics, driving differences in NPP and export production, and contributing to
134 intramodel variability in projections of the BCP.

135

136 2. Methodology

137

138 2.1 PISCES configurations

139

140 Tab. (1) presents a summary of the five PISCES configurations used in this study, which differ
141 primarily in their parameterisation of phytoplankton growth processes. The standard PISCES (PST)
142 model of Aumont et al. (2015) served as the foundation for all configurations. The PST model
143 simulates the lower trophic levels of marine ecosystems and resolves the biogeochemical cycles of
144 carbon and the main nutrients of P, N, Si and Fe. The model has four living compartments, two
145 phytoplankton functional types (PFTs; diatoms and nanophytoplankton) and two zooplankton size
146 classes (microzooplankton and mesozooplankton). Particulate detritus, produced through
147 phytoplankton–zooplankton–nutrient interactions, is partitioned into small and large particles. Both
148 size classes arise from multiple processes, including zooplankton grazing, phytoplankton and
149 zooplankton mortality, and aggregation. However, their dominant sources differ as small particles
150 are primarily linked to nanophytoplankton–microzooplankton interactions, whereas large particles
151 are mainly associated with those of diatom–mesozooplankton. The PST model employs a hybrid of
152 Monod-quota formulations in representing the cycling of major nutrients. Phytoplankton C:N:P



153 stoichiometry is fixed, with N and P limitations governed by a Monod parameterisation. As a result,
 154 growth rates follow a rectangular hyperbolic function of the limiting external nutrient concentration
 155 (Monod, 1949; Flynn, 2003). In contrast, Fe limitation is represented with a quota-based approach
 156 (Aumont et al., 2015), where growth depends on the internal nutrient quota of a cell, which itself is
 157 regulated by the external nutrient concentration (Droop, 1968).

158

159 Table 1: List of PISCES configurations

160

Configuration name	Short name	Nutrients	Phytoplankton types	Phytoplankton growth	Additional parameterisations relative to PST	References
PISCES standard	PST	P, N, Fe, Si	Nano-, diatom	Monod & quota (Fe)	Standard	Aumont et al. (2015); Tagliabue et al. (2020)
					$\theta^{Fe,I}; \theta_{max}^{Fe,I}$	
PISCES low-Fe	PSF	P, N, Fe, Si	Nano-, diatom	Monod & quota (Fe)	The biological ($\theta^{Fe,I}$) and maximum ($\theta_{max}^{Fe,I}$) iron quotas (umol Fe/mol C) for the two phytoplankton groups are adjusted for low iron conditions.	Tagliabue et al. (2020)
					$f^n = 1 - \frac{Q_q^n}{Q^n}$	
PISCES-QUOTA	P5Z	P, N, Fe, Si	Nano-, pico-, diatom	Quota	f^n is the effect of a given nutrient on phytoplankton growth rate, Q^n is the internal ratio of nutrient n to carbon biomass, and Q_q^n is the subsistence or minimum quota of the respective nutrients.	Kwiatkowski et al. (2018); Wrightson et al. (2022)
PISCES diazotroph (tricho)	P6Z	P, N, Fe, Si	Nano-, pico-, diatom, diazotroph	Quota	The addition of a diazotroph PFT to represent <i>Trichodesmium</i> . Thermal performance curves modulate diazotroph maximum growth rate and the elemental use efficiency (EUE) of P and Fe.	Wrightson et al. (2022)
PISCES Manganese	P5M	P, N, Fe, Mn, Zn, Si	Nano-, pico-, diatom	Quota	The inclusion of the biogeochemical Mn cycle and phytoplankton Mn limitation. The limiting nutrients for diatoms include: N, P, Si, Fe, Zn and Mn.	Anugerahanti and Tagliabue (2023, 2024)

161

162 The PST and low-Fe PISCES (PSF) configurations are those described in Tagliabue et al. (2020).
 163 The PSF configuration modified PST by adjusting biological and maximum iron quotas for
 164 phytoplankton growth to better reflect low-iron conditions and their implications under climate
 165 change. Iron availability plays a key role in regulating phytoplankton growth and global NPP
 166 (Tagliabue et al., 2017); however, ESMs often show large uncertainties in representing the ocean
 167 iron cycle and its effect on productivity (Tagliabue et al., 2016). Unlike PST and PSF, the
 168 PISCES-QUOTA (P5Z) model allows for variable C:N:P stoichiometry (Kwiatkowski et al., 2018),
 169 with growth exclusively governed by quota-based formulations (Tab. 1). P5Z resolves 39 prognostic
 170 variables, compared to 24 in PST, and importantly includes three phytoplankton groups:
 171 picophytoplankton, nanophytoplankton, and diatoms.

172



173 Wrightson et al. (2022) further developed the model by introducing an explicit diazotroph PFT
174 (*Crocospaera* and *Trichodesmium*), along with temperature-dependent nutrient uptake
175 parameterised via elemental use efficiencies (EUEs), resulting in the P6Z configuration. These
176 additions addressed a key limitation in P5Z, which represented nitrogen fixation as an implicit flux
177 of ammonia, preventing mechanistic investigation of diazotroph dynamics. Given that marine
178 nitrogen fixation plays a critical role in shaping the response of NPP to climate change (Wrightson
179 and Tagliabue, 2020; Bopp et al., 2022), explicitly resolving diazotrophs in P6Z allowed responses
180 to environmental drivers, especially rising ocean temperatures, to be investigated. Preliminary work
181 conducted in this study showed little difference in global C_{exp} or NPP patterns across the various
182 P6Z versions in Wrightson et al. (2022). Therefore, in this study, we used only the configuration
183 that included temperature dependent EUEs for Fe and P for the generic N-fixing PFT (Tab. 1).

184

185 Anugerahanti and Tagliabue (2024) built upon the base P5Z model by incorporating manganese
186 (Mn), following Hawco et al. (2022), which included its role in limiting phytoplankton productivity
187 in the Southern Ocean, where observations show Mn as either a primary or co-limiting
188 micronutrient alongside Fe (Wu et al., 2019; Browning et al., 2021; Hawco et al., 2022). The
189 resulting P5M configuration explicitly simulates coupled Mn and zinc (Zn) cycles (Richon and
190 Tagliabue, 2021), including biological uptake, scavenging, and regeneration for Mn and Zn.

191

192 The various PISCES configurations (Tab. 1) were identically forced with physical outputs from the
193 [IPSL-CM5A-LR](#) climate model on the ORCA tripolar grid with 2° horizontal spatial resolution.
194 Two model runs were conducted for each configuration. The first simulation was forced by outputs
195 derived from historical (1851-2005) climate forcing and the second with the high emission
196 Representative Concentration Pathway 8.5 (RCP8.5) scenario (2006-2100). For this study, we
197 conducted our analysis of the BCP using averaged model outputs over two time windows, the
198 'reference' (1986-2005) and 'future' (2091-2100).

199

200 2.2 Remote-sensing products

201

202 The five PISCES configurations were assessed for the reference period against an ensemble of
203 satellite-derived NPP and C_{exp} products, averaged over 1998-2005. This period was chosen to align
204 with the model simulations while accommodating the earliest availability of satellite observations.
205 Model outputs and remote-sensing products were compared globally as well as across RECCAP2
206 biomes (Supp. S1) by ocean basin (Fay and Mckinley, 2014; Doney et al., 2024).

207

208 Several algorithms have been described to estimate primary production based on ocean-colour
209 remote-sensing observations, each differing in complexity and formulation and exhibiting
210 substantial variability across regions such as the subtropical gyres and the Southern Ocean
211 (Ryan-Keogh et al., 2023; Westberry et al., 2023). Common algorithms include the: Vertically
212 Generalised Production Model (VPGM), Carbon-based Production Model (CbPM), and Carbon
213 Absorption Fluorescence Euphotic-resolving (CAFE) model. This study used six different NPP
214 datasets (Supp. S2), all of which are derived from ESA Ocean Colour Climate Change Initiative
215 (OC-CCI) remotely-sensed chlorophyll concentrations (Sathyendranath et al., 2019). Five were
216 from the regular 25 km gridded NPP datasets at 8-day resolution of Ryan-Keogh et al. (2023), who
217 considered the Eppley-VGPM (Eppley 1972), Behrenfeld-VGPM (Behrenfeld and Falkowski, 1997),
218 Behrenfeld-CbPM (Behrenfeld et al., 2005), Westberry-CbPM (Westberry et al., 2008), and the
219 Silsbe-CAFE model (Silsbe et al., 2016). The sixth NPP dataset was the 9 km monthly resolution
220 product from the Biological Pump and Carbon Exchange Processes (BICEP) project (Kulk et al.,
221 2020, 2021) which used a modified version of the base algorithm of Longhurst et al. (1995).

222



223 Similar to NPP, a number of algorithms exist to compute C_{exp} from remotely-sensed observations
 224 (Jönsson et al., 2023). Export production can be related to NPP through a simple scaling factor
 225 (Eppley and Peterson, 1979) or include multiple relationships, such as mixed-layer depth (MLD),
 226 chlorophyll and SST (Jönsson et al., 2023). For simplicity, we restricted our analysis to export
 227 algorithms that estimate C_{exp} from empirical relationships between NPP and SST. We applied five
 228 commonly used formulations (Supp. S3, S4): Laws et al. (2000), Henson et al. (2011), two
 229 equations from Laws et al. (2011), and Li and Cassar (2016). These algorithms have been evaluated
 230 against *in situ* observations (e.g. Dunne et al., 2005; Mouw et al., 2016; Bisson et al., 2018), with
 231 reported skill scores of $R^2 = 0.64\text{--}0.70$ (Li and Cassar, 2016; Jönsson et al., 2023). It is important to
 232 note that they estimate export at different depth horizons such as Henson et al. (2011) at 100 m and
 233 Li and Cassar (2016) at the climatological MLD, meaning biases in subtropical gyres and polar
 234 regions may differ slightly across algorithms. We used SST from the 0.05° Operational Sea Surface
 235 Temperature and Sea Ice Analysis (OSTIA) product, which is a Level 4 product that combines
 236 multi-sensor satellite and *in situ* data (Good et al., 2020). From the daily fields for 1998–2005,
 237 monthly SST averages were computed for OSTIA. Thereafter, C_{exp} was computed using the five
 238 algorithms applied to the monthly SST and six NPP fields (interpolated to the 2° model grid),
 239 resulting in 30 individual C_{exp} estimates. For each algorithm, outputs from the six datasets were then
 240 averaged to produce a single representative C_{exp} field, yielding five ensemble algorithm outputs
 241 (Supp. S3).

242

243 3. Results

244

245 3.1 Model and remote-sensing variability

246

247 Table 2: Reference and future projections of NPP, C_{exp} , and e-ratio for the five PISCES configurations. C_{exp} is
 248 defined as the mass of POC sinking through the 100 m depth horizon, consistent with CMIP conventions
 249 (Palevsky and Doney, 2018). The e-ratio (C_{exp}/NPP) reflects the efficiency of the BCP as governed by
 250 particle formation and sinking processes. NPP is integrated over the upper 100 m when calculating the
 251 e-ratio. NPP and C_{exp} are reported as globally integrated values (Pg C yr^{-1}), and the e-ratio as an
 252 area-weighted global mean. Relative changes (%) from the reference to future period are shown, alongside
 253 CMIP5 estimates from Fu et al. (2016) and remote-sensing (RMT) values from this study's ensemble and
 254 Doney et al. (2024).

255

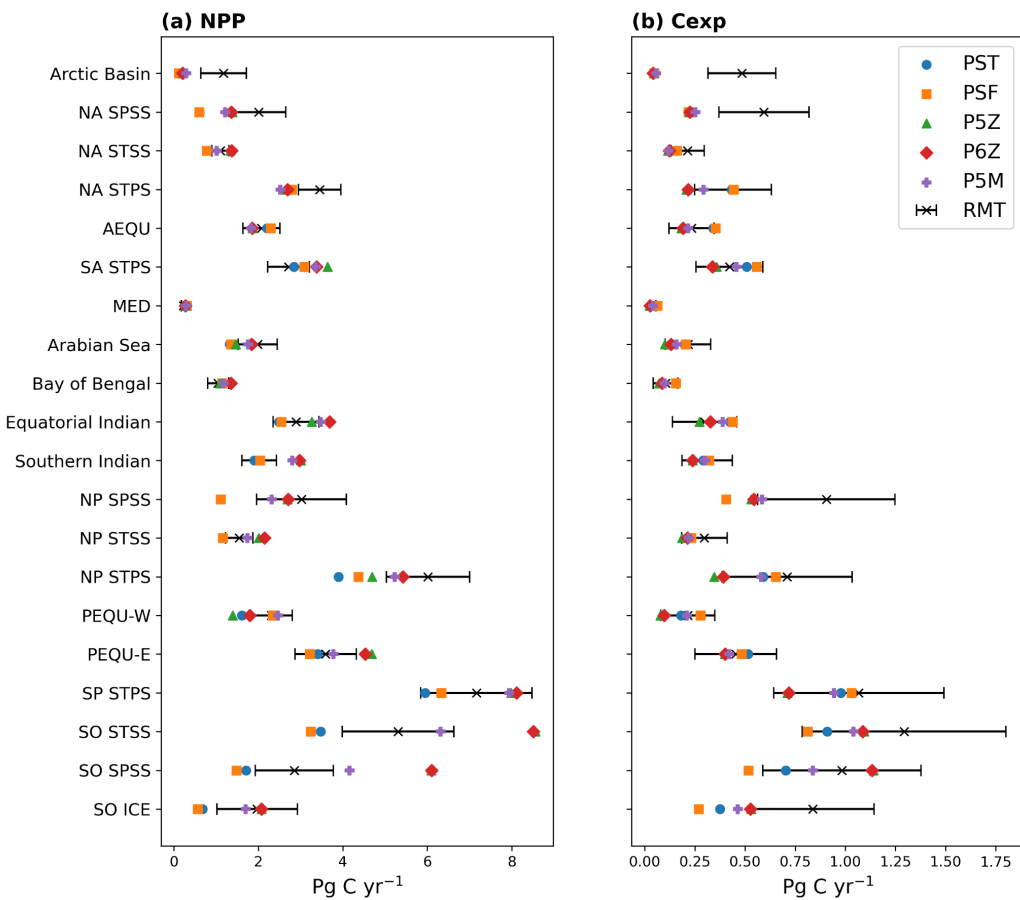
	Reference			Future			Relative change		
	NPP	C_{exp}	e-ratio	NPP	C_{exp}	e-ratio	NPP	C_{exp}	e-ratio
PST	40.78	7.92	0.26	39.44	7.03	0.26	-3.29	-11.23	~ 0
PSF	42.3	7.85	0.24	40.93	6.97	0.24	-3.24	-11.21	~ 0
P5Z	61.15	6.91	0.14	54.92	5.88	0.14	-10.19	-14.91	~ 0
P6Z	63.29	7.12	0.14	58.69	6.13	0.13	-7.27	-13.90	-7.14
P5M	57.11	7.88	0.17	52.81	6.82	0.17	-7.53	-13.36	~ 0
Mean	52.93±10.64	7.54±0.48	0.19±0.057	49.36±8.65	6.57±0.53	0.19±0.059	-6.30±3.00	-12.94±1.65	-1.43±3.19
CMIP5 - Fu et al. (2016)	46.33±13.74	6.17±0.87	0.14±0.041	43.73±14.84	5.40±0.77	0.13±0.037	-6.55±4.19	-12.50±3.78	-6.33±3.64
RMT - study ensemble	55.99±9.95	10.43±3.74	-	-	-	-	-	-	-
RMT - Doney et al. (2024)	52.9±9.1	8.20±2.78	0.196±0.106	-	-	-	-	-	-

272 At both the global (Tab. 2) and biome scales (Fig. 1), differences in the complexity of
 273 phytoplankton processes and parameterisations (Tab. 1) among the five PISCES configurations



274 leads to substantial intramodel variability in both the reference and future states (Figs. 2-3),
 275 particularly for NPP. For the reference period (Tab. 2), the coefficient of variation (CV) for global
 276 NPP across the five configurations is $\sim 20\%$, indicating substantial divergence among models.

277



278

279 Figure 1: Model and remote-sensing (RMT) estimates of (a) NPP and (b) C_{exp} , integrated over each
 280 RECCAP2 biome. Black bars indicate ± 1 standard deviation across the remote-sensing ensemble.

281

282 The two Monod-quota configurations, PST and PSF, simulate 15-21 Pg C yr^{-1} less NPP than the
 283 purely Quota-based configurations (P5Z, P6Z and P5M). In contrast, the relative range of C_{exp} is
 284 much lower ($\text{CV} \approx 5\%$), showing export production is far more consistent across configurations and
 285 reflecting the fact that no direct adjustments were made to the equations or parameterisations
 286 explicitly controlling carbon export across the different configurations. Variability arises as an
 287 indirect outcome, emerging primarily from upstream differences in primary productivity patterns,
 288 which cascade down to influence export. Collectively, this results in the Monod-quota
 289 configurations resolving a more efficient BCP than the purely Quota-based ones. However, despite
 290 these intramodel differences, all the PISCES configurations largely fall within the range of
 291 remote-sensing estimates for both NPP and C_{exp} (Tab. 2). Compared to the CMIP5 ensemble, NPP
 292 for the PISCES configurations lies within the range of variability, whereas C_{exp} exceeds the upper
 293 bound.

294



295 At the biome scale (Fig. 1), no single configuration consistently reproduces all regions, with
296 intramodel variability in NPP (Fig. 1a) and C_{exp} (Fig. 1b) varying considerably. A similar state of
297 variability exists for remote-sensing derived estimates. The Southern Ocean shows the strongest
298 intramodel variability ($CV \geq 30\%$; Supp. S5). P5Z and P6Z yield the highest NPP and C_{exp} , while
299 the Monod-quota models give the lowest. P5M stands apart from both groups, with the inclusion of
300 the manganese cycle dampening phytoplankton growth in this region, resulting in lower NPP than
301 the other Quota-based configurations. This reduction in productivity propagates downstream,
302 ultimately leading to lower C_{exp} . In the equatorial and subtropical gyres, the Quota-based
303 configurations simulate higher NPP, yet the simpler Monod-quota models produce slightly higher
304 C_{exp} , indicating that greater primary production does not directly translate into greater export in
305 these regions (see also Fig. 2). The inclusion of a diazotroph PFT in P6Z introduces regional
306 differences relative to P5Z within these biomes, most notably in the South Atlantic and North
307 Pacific subtropical gyres; however, C_{exp} remains broadly similar between the two configurations
308 (Fig. 1b). The absence of a uniform NPP response to the added diazotroph group reflects
309 basin-specific nutrient limitation regimes, particularly differences in Fe and P availability that
310 constrain diazotroph growth across ocean basins (Wrightson et al., 2022). For PSF, the low-iron
311 biological parameterisation results in slightly higher NPP in the equatorial biomes and subtropical
312 gyres, but marginally lower productivity in the Southern Ocean compared to PST. This occurs
313 because PSF prescribes smaller Fe:C quotas for phytoplankton, enabling growth under lower iron
314 supply. As a result, productivity in low latitude biomes responds more strongly to assumptions
315 about biological iron uptake, where Fe and N limitation play a larger role, whereas productivity in
316 the Southern Ocean is less affected due to its already pervasive iron limitation (Tagliabue et al.,
317 2020).

318

319 3.2 Future projections of the BCP

320

321 From Tab. (2), all configurations project future global declines in both NPP and C_{exp} by 2100, with
322 NPP decreasing by $6.30 \pm 3.00\%$ and C_{exp} by $12.94 \pm 1.65\%$; however, the e-ratio remains largely
323 unchanged. The relatively stable e-ratio indicates that BCP efficiency is maintained within each
324 configuration, but the overall decline in carbon export reduces the ocean's capacity to sequester CO₂
325 from the atmosphere. For NPP and C_{exp} , the largest absolute and relative declines are observed in
326 the Quota-based configurations but all configurations fall within the variability of the CMIP5
327 ensemble (Tab. 2).

328

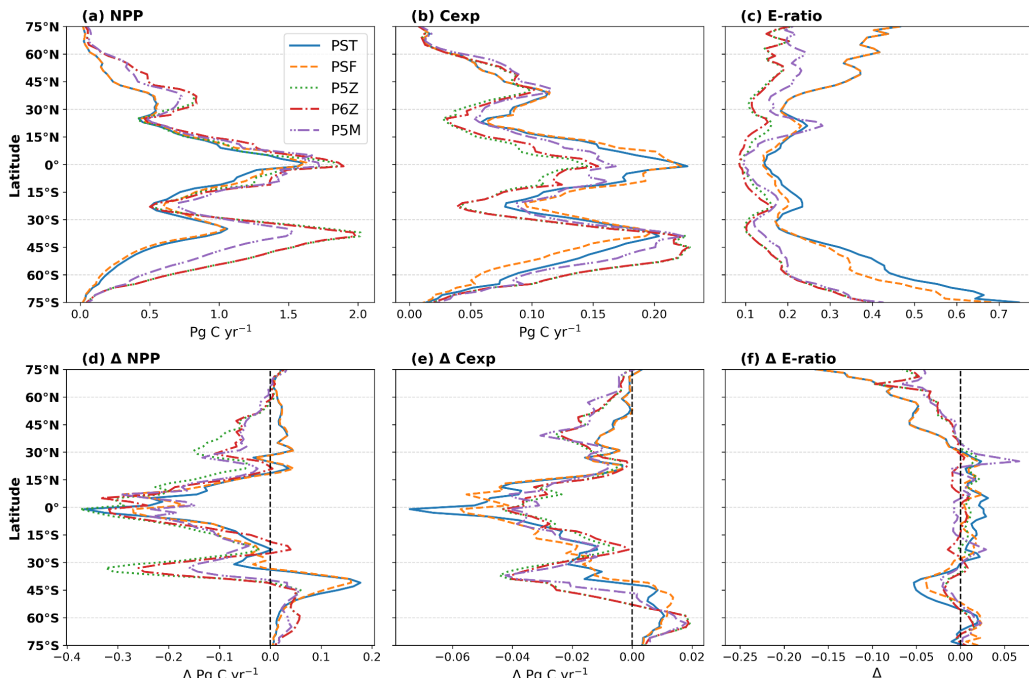
329 Fig. (2) expounds on the biome scale assessment in Fig. (1), presenting zonally integrated NPP and
330 C_{exp} , and area-weighted e-ratios for the reference period, along with their projected future changes.
331 For the reference period (Fig. 2a-c), all configurations reproduce the expected pattern of elevated
332 NPP and C_{exp} in the equatorial region and at high latitudes, including the Southern Ocean and the
333 subpolar to polar regions of the Northern Hemisphere, with lower values in the subtropical gyres.
334 Differences arise mainly in magnitude, with the Quota-based configurations simulating higher NPP
335 than the simpler Monod-quota ones (Fig. 2a); however, this does not translate into uniformly higher
336 C_{exp} (Fig. 2b), resulting in a less efficient BCP (Fig. 2c). Intramodel variability in C_{exp} is less than
337 NPP, with PST and PSF producing slightly higher export production between $\sim 20^\circ$ N/S but notably
338 lower C_{exp} than the Quota-based configurations in the Southern Ocean ($40\text{--}75^\circ$ S).

339

340 For future projections (Fig. 2d-f), all configurations simulate declining NPP between 30° N/S (Fig.
341 2d). Beyond this band, the models diverge. Around 45° S, PST and PSF show an increase in NPP of
342 $\sim 25\%$, whereas the Quota-based configurations show only a 4-5% rise. North of 30° N, the
343 Monod-quota configurations exhibit increasing NPP (from $\sim 1\%$ to 20% by 60° N), while the
344 Quota-based configurations instead show a sharp decline of 15-25% at 30° N, which gradually



345 weakens poleward. All configurations eventually project higher NPP in the northern polar region
 346 (Fig. 2d). In contrast, future changes in C_{exp} (Fig. 2e) follow a broadly consistent pattern across
 347 configurations, differing mainly in magnitude rather than trajectory. All configurations show
 348 declining export production over most latitudes, with a regional exception in the Southern Ocean,
 349 where C_{exp} increases. This increase occurs farther north ($\sim 45^\circ$ S) in PST and PSF, reflecting their
 350 distinct NPP response, while the Quota-based models show a similar feature centred farther south.
 351 North of 30° N, all configurations show declining C_{exp} , though the strength of the reduction varies
 352 Collectively, the e-ratio remains relatively stable across latitudes, with no clear model-specific
 353 pattern between 30° N/S (Fig. 2f). All models show a 10-20% decline in the e-ratio near 45° S, an
 354 increase of ~ 5 -10% south of 60° S, and a consistent decrease north of 30° N (Fig. 2f).



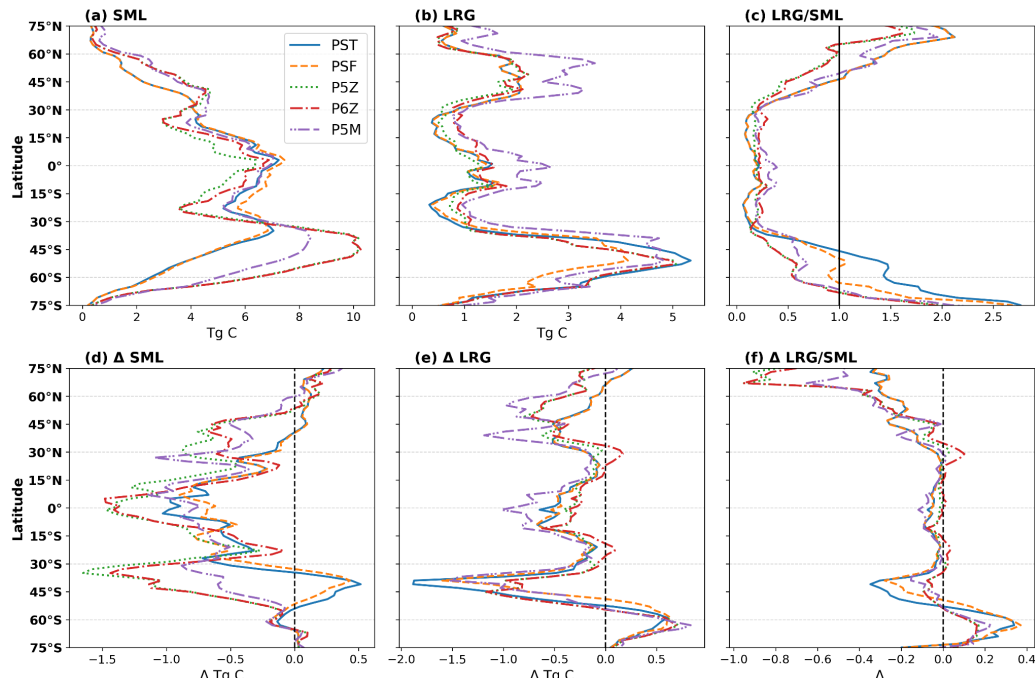
355
 356 Figure 2: Top row shows zonally integrated (a) NPP and (b) C_{exp} , and the area-weighted mean (c) e-ratio for
 357 the reference period. The lower row (d-f) shows the respective changes in the future relative to the reference
 358 period.

359 Intramodel variability in NPP, C_{exp} , and e-ratio across the reference and future periods reflects both
 360 the direct effects of differing phytoplankton parameterisations (Tab. 1) and the cascading, top-down
 361 consequences of these choices. To interpret the latitudinal patterns in Fig. (2), it is necessary to
 362 examine how phytoplankton biomass responds within each configuration. Accordingly, Fig. (3)
 363 shows the reference and relative future changes in total phytoplankton biomass, grouped into small
 364 (SML) and large (LRG) phytoplankton to accommodate differences in PFT structure across
 365 configurations.

366
 367 For the reference period (Fig. 3a-c), the spatial patterns and intramodel differences in small (Fig.
 368 3a) and large (Fig. 3b) phytoplankton biomass closely parallel those of NPP (Fig. 2a) and C_{exp} (Fig.
 369 2b). These patterns are expected and stem from the differing ecological functions and
 370 environmental sensitivities of small versus large phytoplankton in the model. Small phytoplankton



371 dominate most of the ocean ($LRG/SML < 1$; Fig. 3c) but contribute little to export because they
 372 remain in the surface layer, whereas large phytoplankton form larger, faster-sinking particles that
 373 disproportionately drive carbon export (Aumont et al., 2015). A striking feature is the substantially
 374 higher biomass of large phytoplankton (Fig. 3b) in P5M relative to the other configurations,
 375 particularly in the equatorial region and north of 30° N. Because P5M was specifically tuned to
 376 represent Mn and other co-limiting trace-metal effects in the Southern Ocean, its divergence
 377 elsewhere likely reflects model-specific tuning that produces unrealistic behaviour outside that
 378 region. This may also explain why P5M yields slightly higher global C_{exp} (Tab. 2) than the other
 379 Quota-based configurations.



380
 381 Figure 3: Top row shows zonally integrated (a) Small (SML) and (b) Large (LRG) phytoplankton biomass,
 382 and the area-weighted mean (c) LRG/SML ratio for the reference period. Across the different PISCES
 383 configurations, PST and PSF have two PFTs, whereas the Quota-based configurations incorporate three
 384 (P5Z and P5M) and four (P6Z). To enable a comparison of phytoplankton biomasses, PFTs were grouped
 385 into ‘small’ (nano-, pico- and N-fixers) and ‘large’ (diatoms) categories. The lower row (d-f) shows the
 386 respective changes in the future relative to the reference period.
 387

388 Responding to future changes in marine environmental conditions, small and large phytoplankton
 389 show global declines of $7.88 \pm 2.97\%$ and $14.24 \pm 1.82\%$, respectively by 2100. Across
 390 configurations, the latitudinal patterns of future changes in small (Fig. 3d) and large (Fig. 3e)
 391 phytoplankton biomass broadly follow those of NPP and C_{exp} (Fig. 2d, e). Intramodel divergence is
 392 most pronounced for small phytoplankton (Fig. 3d). South of 30° S, PST and PSF show increasing
 393 small phytoplankton biomass toward higher latitudes, whereas the Quota-based configurations
 394 simulate the opposite trend. Around $\sim 40^\circ$ S this contrast is strongest, marking the clearest separation
 395 between the two model frameworks. North of 30° N, the configurations also diverge, with opposing
 396 latitudinal trends between 30 - 60° N. These differences likely stem from the contrasting
 397 phytoplankton complexity (i.e. the number of PFTs) and growth formulations across the



398 Monod-quota and Quota-based configurations, which strongly shape how small phytoplankton, and
399 therefore NPP, respond to future environmental change.

400 Large phytoplankton show comparatively little intramodel variability (Fig. 3e), with all
401 configurations exhibiting similar spatial patterns and future changes, differing mainly in magnitude.
402 The largest deviations occur again in P5M outside the Southern Ocean, reflecting its anomalously
403 high large phytoplankton biomass in the reference state (Fig. 3b). Overall, the LRG/SML ratio is
404 projected to decline globally by $6.83 \pm 3.33\%$, with the largest absolute and relative changes
405 occurring for PST and PSF, especially near $\sim 45^\circ$ and 60° S (Fig. 3f). A declining ratio indicates a
406 shift towards proportionally more small phytoplankton at the global scale, although regional
407 exceptions occur, most notably in parts of the Southern Ocean, where large phytoplankton become
408 locally more dominant (Fig. 3f). Nevertheless, the concurrent global declines in both small and
409 large phytoplankton biomass ultimately reduces future NPP and C_{exp} .

410 4. Discussion

411 4.1 Differences in phytoplankton parameterisations driving intramodel variability

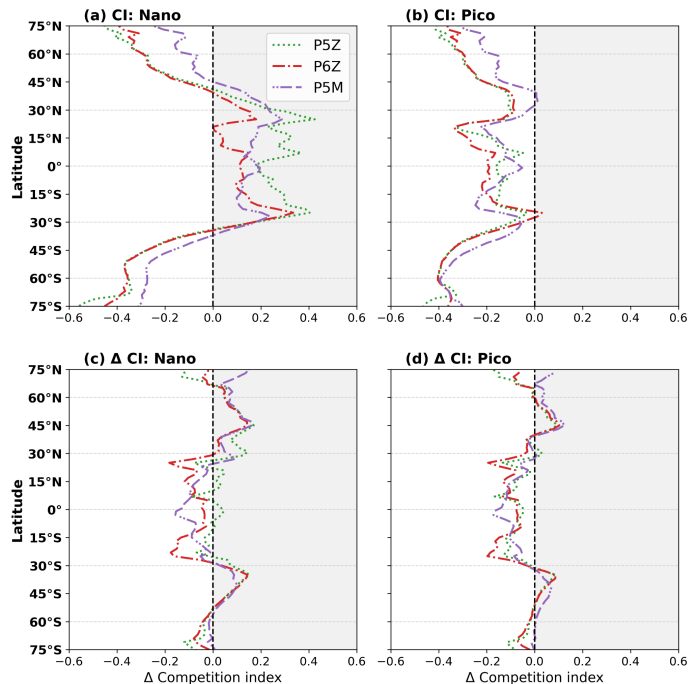
412 Our results show that the more complex Quota-based configurations, which each include some
413 combination of additional PFTs, a more detailed growth formulation, and expanded nutrient
414 cycling, simulate a less efficient BCP than the simpler Monod-quota configurations for both the
415 reference and future periods. For the reference period, the added complexity across the five PISCES
416 configurations produces notable differences at both global (Tab. 2) and biome (Fig. 1) scales, most
417 clearly in NPP. Intramodel variability in C_{exp} is smaller and appears mainly as an indirect
418 consequence of differences in NPP rather than from explicit changes to export related
419 parameterisations. Despite these differences, all configurations reproduce broadly similar
420 large-scale patterns in NPP, C_{exp} , and the distribution of small and large phytoplankton for the
421 reference period, with intramodel differences arising in the magnitude of these respective fields.

422 The more complex Quota-based configurations simulate higher global NPP than the Monod-quota
423 configurations, but this increase does not translate uniformly into higher C_{exp} because the additional
424 productivity is carried by small phytoplankton, which enhance upper-ocean biomass but contribute
425 little to export. From Fig. (2b), export production is greater in PST and PSF between $\sim 20^\circ$ N/S,
426 whereas outside these latitudes, particularly in the Southern Ocean, C_{exp} is highest in the
427 Quota-based models. These contrasting, and in some regions contradictory, patterns in NPP and C_{exp}
428 behaviour for the reference period between the configurations likely arise from top-down controls
429 linked to the greater PFT complexity in the Quota-based configurations and its influence on
430 zooplankton dynamics. These interactions also likely underpin the intramodel differences seen in
431 the future projections of NPP and the BCP.

432 Between the standard model (Aumont et al., 2015) and PISCES-QUOTA, the two biggest updates
433 are the representation of phytoplankton growth processes to use a quota-formulation and the
434 addition of a dedicated picophytoplankton PFT (Kwiatkowski et al., 2018). Furthermore, the
435 zooplankton feeding parameterisations are also adjusted. In the standard PST and PSF
436 configurations, mesozooplankton feed on nanophytoplankton and diatoms, generating large sinking
437 particles via faecal pellet production. In PISCES-QUOTA, however, picophytoplankton are grazed
438 exclusively by microzooplankton rather than mesozooplankton. From this study, it is not possible to
439 fully disentangle the respective contributions of the quota-based growth formulation and the
440 inclusion of additional PFTs to variability in NPP and C_{exp} within the Quota-based configurations.
441 The higher NPP simulated by these configurations (Tab. 2) is partly attributable to their explicit
442 treatment of nitrogen assimilation costs as flexible stoichiometry reduces respiratory losses when



443 ammonium (NH_4^+) is available. This then yields higher effective growth rates than in the
 444 Monod-quota configurations, particularly in low latitudes and during summer at high latitudes.
 445 However, NPP differences between the Monod-quota and Quota-based configurations remain
 446 modest in low latitudes (Fig. 2a), whereas in polar regions, a clearer association emerges between
 447 elevated small phytoplankton biomass and enhanced NPP in the Quota-based configurations.
 448 Kwiatkowski et al. (2018) concluded that accounting for variable phytoplankton stoichiometry has a
 449 limited impact on the global carbon cycle such that the added PFT complexity is likely the primary
 450 parameterisation driving the divergence in behaviour between the Monod-quota and Quota-based
 451 configurations in our study.



452
 453 Figure 4: The competition index (CI) quantifies where the standard nanophytoplankton PFT (mean of PST
 454 and PSF) outperforms the nano- and picophytoplankton PFTs of the Quota-based configurations. CI is
 455 computed from the mean realised growth rates (μ) over the upper 100 m and defined as $\text{CI} = (\mu_1 - \mu_2) / (|\mu_1|$
 456 $+ |\mu_2|)$, where μ_1 is the mean Monod-quota nano- PFT and μ_2 is either the nano- or picophytoplankton PFT
 457 from the Quota-based configurations. Positive values showcase regions where the nanophytoplankton PFT
 458 of the Monod-quota configurations outcompetes the nano- and/or picophytoplankton PFT of the
 459 Quota-based models. Panels show CI for the reference (a, b) period and future shifts (c, d).

460
 461 The competition index (CI; Fig. 4a) shows that the single small nanophytoplankton PFT in the
 462 Monod-quota configurations outcompetes the nanophytoplankton PFT in the Quota-based
 463 configurations across the equatorial and lower-latitude regions, although it is consistently
 464 outcompeted by the picophytoplankton group across all regions (Fig. 4b). Splitting the small
 465 phytoplankton PFT of the standard model into two distinct PFTs in PISCES-QUOTA allows for
 466 greater ecosystem complexity and differentiation across environmental niches. For the open-ocean
 467 regions of the lower latitudes (0-30° N/S), picophytoplankton dominate, comprising 50-70% of total
 468 phytoplankton biomass for the reference period (Supp. 6). Consequently, relative to the
 469 Monod-quota configurations, nanophytoplankton biomass is smaller in the Quota-based
 470 configurations, but this reduction is offset by picophytoplankton biomass, leading to similar overall



471 NPP in the region. However, because mesozooplankton feed exclusively on nanophytoplankton and
472 diatoms, the reduced nanophytoplankton biomass in the Quota-based configurations limits their
473 food supply. This leads to lower mesozooplankton grazing rates (Supp. S7d) and a reduced
474 production of large sinking particles. This mechanistically explains why export production is higher
475 in the equatorial region in PST and PSF compared with the Quota-based configurations (Fig. 2b).

476 Outside of 30° N/S, the CI shows a shift in competitive behaviour, with the nanophytoplankton PFT
477 for the Quota-based configurations now outcompeting the single nanophytoplankton PFT of the
478 Monod-quota models (Fig. 4a). Because picophytoplankton already outcompete the Monod-quota
479 nano- PFT everywhere (Fig. 4b), this means that small phytoplankton as a whole can proliferate
480 more effectively in the Quota-based configurations beyond the tropics. This explains the higher
481 small phytoplankton biomass (Fig. 3a) and elevated NPP (Fig. 2a) in these regions. This pattern is
482 strongest in the Southern Ocean, where the Quota-based configurations show substantially higher
483 NPP and export production compared to PST and PSF. The elevated small phytoplankton biomass
484 fuels enhanced micro- and mesozooplankton grazing rates (Supp. S7c, d), enhancing export
485 production in the Southern Ocean (Fig. 2b) and this mechanism is consistent with the findings of
486 Laufkötter et al. (2013).

487 The mechanistic patterns identified in the reference period provide a critical foundation for
488 understanding why certain regions show stronger divergence than others in the future projections of
489 NPP and the BCP across the PISCES configurations. By 2100, our results show global NPP and
490 C_{exp} are projected to decline by $6.30 \pm 3.00\%$ and $12.94 \pm 1.65\%$, respectively, accompanied by a shift
491 towards dominance of small phytoplankton species. These findings align with previous modelling
492 studies (Bindoff et al., 2019), falling within the variability of the CMIP5 ensemble (Bopp et al.,
493 2013; Fu et al., 2016). The comparable magnitude of variability in NPP and C_{exp} (Tab. 2) indicates
494 that differences in parameterisations among the selected PISCES configurations likely encompass a
495 substantial portion of the intermodel spread in biogeochemical complexity observed across CMIP
496 models (Séférian et al., 2020), suggesting that much of the variability in CMIP may arise from
497 relatively subtle differences in the representation of phytoplankton growth processes and ecosystem
498 complexity.

499
500 Despite global future reductions in NPP and C_{exp} in response to shifting physical marine
501 environmental conditions, the e-ratio shows little to no significant change for the five PISCES
502 configurations, indicating that BCP efficiency is maintained relative to the reference period, but the
503 overall decline in carbon export reduces the ocean's capacity to sequester CO₂ from the atmosphere.
504 In Fig. (4c, d), the CI shows little change between the reference and future periods, indicating that
505 the relative competitive balance among PFTs remains largely unchanged. Consequently, the
506 Quota-based configurations continue to sustain higher absolute NPP in the future (Tab. 2) than the
507 Monod-quota configurations. However, they also maintain lower C_{exp} , reflecting persistent regional
508 differences in phytoplankton-zooplankton interactions (Supp. S7) that stem from the contrasting
509 levels of PFT complexity, particularly within the small phytoplankton community, across the
510 PISCES configurations.

511
512 Intramodel variability is greatest between 30-60° N/S for future projections of NPP and C_{exp} . Small
513 phytoplankton biomass increases from 30° S to a peak near ~40° S in the Monod-quota
514 configurations before weakening toward 60° S, whereas the Quota-based configurations show the
515 opposite latitudinal pattern, with both model families converging at ~60° S (Fig. 3d). NPP responds
516 accordingly, though the impact on C_{exp} is more muted. Under future changes in marine
517 environmental conditions, such as warmer SSTs and enhanced stratification, the simpler
518 Monod-quota models project an increase in small phytoplankton biomass, whereas the Quota-based
519 configurations project a decline in this region. This divergence arises from the added phytoplankton



520 complexity in the Quota-based configurations. By explicitly representing picophytoplankton, P5Z,
521 P6Z, and P5M resolve a broader range of ecological niches. As marine environmental conditions
522 shift, the response of picophytoplankton dominates the overall behaviour of the small
523 phytoplankton community, leading to a decrease in biomass (Fig. 3d). In contrast, the single
524 nanophytoplankton PFT in the Monod-quota models, being more generalised and arguably
525 over-parameterised, responds differently and shows an increase for 30–60° S. A similar pattern
526 emerges in the Northern Hemisphere, where both model families project an overall decline in small
527 phytoplankton biomass but the latitude-dependent trends differ (Fig. 3d). Again, this reflects the
528 distinct niche sensitivities of the picophytoplankton PFT in the Quota-based configurations versus
529 the more simplified single nanophytoplankton PFT present in the Monod-quota configurations.

530

531 4.2 Complexity and the persistence of uncertainty

532

533 For both the reference and future periods, our results show that differences in biogeochemical
534 parameterisations constitute a major axis of divergence across the five PISCES configurations.
535 Importantly, not all parameterisations exert influence at the same scale. Some, such as the
536 introduction of the picophytoplankton PFT in PISCES-QUOTA, generates substantial shifts in
537 global NPP, which in turn leads to moderate but consistent differences in C_{exp} , for both the reference
538 and future periods relative to the Monod-quota configurations. Other parameterisations exert more
539 limited effects, such as low-iron parameterisation in PSF, added diazotroph PFT in P6Z, and explicit
540 manganese cycling for P5M, impacting phytoplankton growth rates or expanding phytoplankton
541 complexity in ways that manifest significant differences in NPP and C_{exp} behaviour at the biome
542 scale rather than globally. Together, our findings highlight that certain parameterisations
543 fundamentally reshape model behaviour, whereas others provide more subtle or regionally confined
544 refinements.

545

546 Added complexity in biogeochemical models is intended to improve the representation of marine
547 ecosystem functioning. However, the current uncertainty ranges in remote-sensing estimates of
548 global NPP and C_{exp} remain extremely large at 46.3% and 109.8%, respectively (Doney et al.,
549 2024). As shown in Fig. (1), all five PISCES configurations fall well within the spectrum of
550 remote-sensing estimates at the biome scale such that understanding whether the added complexity
551 is improving representation of the marine system is difficult to discern. Although not the focus of
552 the study, a skill assessment of the different configurations relative to the ensemble mean of the
553 various remote-sensing NPP and C_{exp} datasets showed no clear or significant improvement in model
554 skill with increasing model complexity for the reference period (Supp. S8). This raises an important
555 point, one that is actively discussed within the modelling community, determining the optimal
556 balance of model complexity, and the most effective combination of parameterisations, when
557 utilising biogeochemical models for future projections of the carbon cycle and the BCP.

558

559 One may argue that more complex biogeochemical models permit more sources of error and
560 degrees of freedom; however, Flynn (2010) makes the bold statement that models that ignore key
561 biogeochemical processes are inherently dysfunctional. Especially for future projections beyond the
562 extent of observations as the absence of process driven biogeochemical feedback will lead to
563 compensating errors and large future uncertainties. Furthermore, one also needs to consider the
564 computational expenses that accompany greater complexity as PISCES-QUOTA is far more costly
565 to operate than the simpler standard model (Kwiatkowski et al., 2018). These *quid pro quos*
566 preclude a single ‘best’ configuration, but they illuminate the key considerations when choosing
567 among PISCES configurations of differing complexity. Finally, we tested these different
568 configurations under the very strong climate forcing of the RCP8.5 scenario. Results may be
569 different under weaker levels of global warming currently expected or strongly mitigated scenarios.



570 **5. Conclusion**

571

572 In this study, we used five distinct PISCES configurations of varying complexity that differ in their
573 number of PFTs, growth formulations, imposed nutrient limitations, and the representation of
574 nutrient cycling. We showed that these parameterisation differences alone can generate substantial
575 divergence and intramodel variability under the high emissions RSP8.5 scenario in projections of
576 the BCP, with NPP responding more sensitively than C_{exp} . Yet, despite these contrasts, all
577 configurations produce for the reference period NPP and C_{exp} magnitudes that fall within the broad
578 range of remote-sensing estimates, making it difficult to assess whether added complexity
579 unequivocally improves model realism. Moreover, the spread in future NPP and C_{exp} projections
580 across the PISCES configurations is comparable to that seen in the CMIP5 ensemble, suggesting
581 that relatively subtle differences in phytoplankton processes and their parameterisation may
582 underpin a substantial fraction of the intermodel variability in ESM projections.

583

584 The introduction of a picophytoplankton PFT in PISCES-QUOTA, and its presence in the other
585 Quota-based configurations, emerges as one of the most influential parameterisation choices,
586 producing higher global NPP yet slightly lower C_{exp} , and driving opposing future NPP responses
587 and latitudinal trends in C_{exp} between 30-60° N/S compared with the Monod-quota configurations.
588 Other parameterisations, such as the low-iron scheme in PSF, the added diazotroph PFT in P6Z, and
589 explicit manganese cycling in P5M, exert more modest, regionally confined effects, influencing
590 NPP and C_{exp} primarily at biome scales rather than driving large-scale divergence in model
591 behaviour. Finding that differing parameterisations produce contrasting model outputs is
592 unsurprising, but the nature of our study allowed us to identify which parameterisations generate
593 substantial intramodel variability and which exert only minimal influence. The discrete number of
594 configurations inevitably constrains our conclusions to parameterisations centred on phytoplankton
595 processes. Nevertheless, within the PISCES and broader ESM modelling community, this study
596 represents a novel contribution, highlighting how different configurations of a biogeochemical
597 model behave in projecting contemporary and future states of NPP and C_{exp} .

598

599

600 **Code availability**

601

602 The code to do the calculations and generate the main manuscript figures can be found at
603 https://github.com/RGRJON002/Complexity_in_Biogeochemical_Models_BCP_Rogerson.git

604

605 **Data availability**

606

607 The remote-sensing data products used in this study are publicly available. The BICEP NPP (<https://doi.org/10.3390/rs12050826>),
608 datasets of Ryan-Keogh *et al.* (2023) (<https://doi.org/10.5281/ZENODO.8314348>), and OSTIA SST
609 (<https://doi.org/10.48670/moi-00168>) can be sourced from the links provided. Model outputs from the different PISCES
610 configurations are available either through direct correspondence with the respective lead authors or via the repository links provided
611 in their associated publications.

612

613 **Author contributions**

614

615 **Conceptualization:** JR, AT, MV, MG **Methodology:** JR, AT, AN, AO, MG **Formal analysis:** JR, AN **Writing-Original Draft:**
616 JR **Data curation:** JR, AT, LW, PA **Writing-Review & Editing:** JR, AT, MV, LW, PA, AO, MG **Funding acquisition:** MG

617

618 **Competing interests**

619

620 The authors declare that they have no conflicts of interest

621

622 **Declaration of AI**

623

624 No generative AI was used in the writing of this manuscript.

625

626



627 **Acknowledgements**

628

629 This project has received funding from the European Union's Horizon 2020 research and innovation programme under grant
630 agreement No. 862923. A portion of the result's section was presented at the 2025 OceanICU Annual Meeting. MG was funded by
631 the European Union under grant agreement No. 101083922 (OceanICU). Views and opinions expressed are however those of the
632 author(s) only and do not necessarily reflect those of the European Union or European Research Executive Agency. Neither the
633 European Union nor the granting authority can be held responsible for them. This work benefited from discussions during the PISCO
634 conference (25-26 September 2025). Special thanks are given to Robbie Norfolk, Lulu White and Betty White. Finally, this
635 manuscript is dedicated to the memory of Lulu, miss you lots.

636

637 **6. References**

638

639 Anugerahanti, P., and Tagliabue, A.: Process controlling iron–manganese regulation of the Southern Ocean biological
640 carbon pump, *Philos. T. R. Soc. A.*, 381(2249), p.20220065, <https://doi.org/10.6084/m9.figshare.c.6486290>, 2023.

641

642 Anugerahanti, P., and Tagliabue, A.: Response of Southern Ocean resource stress in a changing climate, *Geophys. Res.*
643 *Lett.*, 51(10), p.e2023GL107870, <https://doi.org/10.1029/2023GL107870>, 2024.

644

645 Aumont, O., Éthé, C., Tagliabue, A., Bopp, L., and Gehlen, M.: PISCES-v2: an ocean biogeochemical model for carbon
646 and ecosystem studies, *Geosci. Model Dev.*, 8, 2465–2513, <https://doi.org/10.5194/gmd-8-2465-2015>, 2015.

647

648 Basu, S., and Mackey, K.R.: Phytoplankton as key mediators of the biological carbon pump: Their responses to a
649 changing climate, *Sustainability*, 10(3), 869, <https://doi.org/10.3390/su10030869>, 2018.

650

651 Behrenfeld, M.J., and Falkowski, P.G.: Photosynthetic rates derived from satellite-based chlorophyll concentration,
652 *Limnol. Oceanogr.*, 42(1), 1–20, <https://doi.org/10.4319/lo.1997.42.1.0001>, 1997.

653

654 Behrenfeld, M.J., Boss, E., Siegel, D.A., and Shea, D.M.: Carbon-based ocean productivity and phytoplankton
655 physiology from space, *Global Biogeochem. Cy.*, 19(1), 1–14, <https://doi.org/10.1029/2004GB002299>, 2005.

656

657 Benedetti, F., Vogt, M., Elizondo, U.H., Righetti, D., Zimmermann, N.E., and Gruber, N.: Major restructuring of marine
658 plankton assemblages under global warming, *Nat. Commun.*, 12(1), 5226, <https://doi.org/10.1038/s41467-021-25385-x>,
659 2021.

660

661 Berzaghi, F., Pinti, J., Aumont, O., Maury, O., Cosimano, T., and Wisz, M.S.: Global distribution, quantification and
662 valuation of the biological carbon pump, *Nat. Clim. Change*, 15, 385–392, <https://doi.org/10.1038/s41558-025-02295-0>,
663 2025.

664

665 Bindoff, N.L., Cheung W.W.L., Kairo, J.G., Arístegui, J., Guinder, V.A., Hallberg, R., Hilmi, N., Jiao, N., Karim, M.S.,
666 Levin, L., O'Donoghue, S., Purca Cuicapsa, S.R., Rinkevich, B., Suga, T., Tagliabue, A., and Williamson, P.:
667 Changing Ocean, Marine Ecosystems, and Dependent Communities, in: *IPCC Special Report on the Ocean and*
668 *Cryosphere in a Changing Climate*, edited by: Pörtner, H.O., Roberts, D.C., Masson-Delmotte, V., Zhai, P., Tignor, M.,
669 Poloczanska, E., Mintenbeck, K., Alegria, A., Nicolai, M., Okem, A., Petzold, J., Rama, B., and Weyer, N.M.,
670 Cambridge University Press, Cambridge (UK) & New York (NY, USA), 447–587,
671 <https://doi.org/10.1017/9781009157964.007>, 2019.

672

673 Bisson, K.M., Siegel, D.A., DeVries, T., Cael, B.B., and Buesseler, K.O.: How data set characteristics influence ocean
674 carbon export models', *Global Biogeochem. Cy.*, 32(9), 1312–1328, <https://doi.org/10.1029/2018GB005934>, 2018.

675

676 Bopp, L., Aumont, O., Cadule, P., Alvain, S., and Gehlen, M.: Response of diatoms distribution to global warming and
677 potential implications: A global model study, *Geophys. Res. Lett.*, 32(L19606), 1–4,
678 <https://doi.org/10.1029/2005GL023653>, 2005.

679

680 Bopp, L., Resplandy, L., Orr, J.C., Doney, S.C., Dunne, J.P., Gehlen, M., Halloran, P., Heinze, C., Ilyina, T., Seferian, R.,
681 Tjiputra, J., and Vichi, M.: Multiple stressors of ocean ecosystems in the 21st century: projections with CMIP5
682 models, *Biogeosciences*, 10(10), 6225–6245, <https://doi.org/10.5194/bg-10-6225-2013>, 2013.

683

684 Bopp, L., Aumont, O., Kwiatkowski, L., Clerc, C., Dupont, L., Ethé, C., Séférian, R., and Tagliabue, A.: Diazotrophy as
685 a key driver of the response of marine net primary productivity to climate change, *Biogeosciences*, 19, 4267–4285,
686 <https://doi.org/10.5194/bg-19-4267-2022>, 2022.

687



688 Browning, T.J., Achterberg, E.P., Engel, A., and Mawji, E.: Manganese co-limitation of phytoplankton growth and
689 major nutrient drawdown in the Southern Ocean, *Nat. Commun.*, 12(1), 884,
690 <https://doi.org/10.1038/s41467-021-21122-6>, 2021.

691

692 Buesseler, K.O., Lamborg, C.H., Boyd, P.W., Lam, P.J., Trull, T.W., Bidigare, R.R., Bishop, J.K., Casciotti, K.L.,
693 Dehairs, F., Elskens, M., and Honda, M.: Revisiting carbon flux through the ocean's twilight zone, *Science*, 316(5824),
694 567-570, <https://doi.org/10.1126/science.1137959>, 2007.

695

696 DeVries, T., Yamamoto, K., Wanninkhof, R., Gruber, N., Hauck, J., Müller, J.D., Bopp, L., Carroll, D., Carter, B., Chau,
697 T.T.T., and Doney, S.C.: Magnitude, trends, and variability of the global ocean carbon sink from 1985 to 2018, *Global
698 Biogeochem. Cy.*, 37(10), p.e2023GB007780, <https://doi.org/10.1029/2023GB007780>, 2023.

699

700 Doney, S.C., Mitchell, K.A., Henson, S.A., Cavan, E., DeVries, T., Gruber, N., Hauck, J., Mouw, C.B., Müller, J.D., and
701 Primeau, F.W.: Observational and numerical modeling constraints on the global ocean biological carbon pump, *Global
702 Biogeochem. Cy.*, 38(7), p.e2024GB008156, <https://doi.org/10.1029/2024GB008156>, 2024.

703

704 Droop, M.R.: Vitamin B12 and marine ecology. IV. The kinetics of uptake, growth and inhibition in *Monochrysis
705 lutheri*, *J. Mar. Biol Assoc. UK.*, 48(3), 689-733, <https://doi.org/10.1017/S0025315400019238>, 1968.

706

707 Ducklow, H.W., Steinberg, D.K., and Buesseler, K.O.: Upper ocean carbon export and the biological pump,
708 *Oceanography*, 14(4), 50-58, 2001.

709

710 Dunne, J.P., Armstrong, R.A., Gnanadesikan, A., and Sarmiento, J.L.: Empirical and mechanistic models for the particle
711 export ratio, *Global Biogeochem. Cy.*, 19(GB4026), 1-16, <https://doi.org/10.1029/2004GB002390>, 2005.

712

713 Dunne, J.P., John, J.G., Adcroft, A.J., Griffies, S.M., Hallberg, R.W., Shevliakova, E., Stouffer, R.J., Cooke, W., Dunne,
714 K.A., Harrison, M.J., and Krasting, J.P.: GFDL's ESM2 global coupled climate–carbon earth system models. Part I:
715 Physical formulation and baseline simulation characteristics, *J. Climate*, 25, 6646-6665,
716 <https://doi.org/10.1175/JCLI-D-11-00560.1>, 2012.

717

718 Eppley, R. W.: Temperature and phytoplankton growth in the sea, *Fish. B-NOAA.*, 70(4), 1063-1085, 1972.

719

720 Eppley, R. W., and Peterson, B.J.: Particulate organic matter flux and planktonic new production in the deep ocean,
721 *Nature*, 282(5740), 677-680, <https://doi.org/10.1038/282677a0>, 1979.

722

723 Falkowski, P.G., Barber, R.T., and Smetacek, V.: Biogeochemical controls and feedbacks on ocean primary production,
724 *Science*, 281(5374), 200-206, <https://doi.org/10.1126/science.281.5374.200>, 1998.

725

726 Falkowski, P., Scholes, R.J., Boyle, E.E.A., Canadell, J., Canfield, D., Elser, J., Gruber, N., Hibbard, K., Högberg, P.,
727 Linder, S., and Mackenzie, F.T.: The global carbon cycle: a test of our knowledge of earth as a system, *Science*,
728 290(5490), 291-296, <https://doi.org/10.1126/science.290.5490.291>, 2000.

729

730 Fay, A.R., and McKinley, G.A.: Global open-ocean biomes: mean and temporal variability, *Earth Syst. Sci. Data*, 6(2),
731 273-284, <https://doi.org/10.5194/essd-6-273-2014>, 2014.

732

733 Fennel, K., Mattern, J.P., Doney, S.C., Bopp, L., Moore, A.M., Wang, B., and Yu, L.: Ocean biogeochemical modelling,
734 *Nat. Rev. Methods Primers*, 2(1), 76, <https://doi.org/10.1038/s43586-022-00154-2>, 2022.

735

736 Fisher, B.J., Poulton, A.J., Meredith, M.P., Baldry, K., Schofield, O., and Henley, S.F.: Climate-driven shifts in Southern
737 Ocean primary producers and biogeochemistry in CMIP6 models, *Biogeosciences*, 22(4), 975-994,
738 <https://doi.org/10.5194/bg-22-975-2025>, 2025.

739

740 Flynn, K.J.: Modelling multi-nutrient interactions in phytoplankton; balancing simplicity and realism, *Prog. Oceanogr.*,
741 56(2), 249-279, [https://doi.org/10.1016/S0079-6611\(03\)00006-5](https://doi.org/10.1016/S0079-6611(03)00006-5), 2003.

742

743 Flynn, K.J.: Ecological modelling in a sea of variable stoichiometry: dysfunctionality and the legacy of Redfield and
744 Monod, *Prog. Oceanogr.*, 84(1-2), 52-65, <https://doi.org/10.1016/j.pocean.2009.09.006>, 2010.

745

746 Frémont, P., Gehlen, M., Vrac, M., Leconte, J., Delmont, T.O., Wincker, P., Iudicone, D., and Jaillon, O.: Restructuring
747 of plankton genomic biogeography in the surface ocean under climate change, *Nat. Clim. Change*, 12(4), 393-401,
748 <https://doi.org/10.1038/s41558-022-01314-8>, 2022.



749 Friedlingstein, P., O'sullivan, M., Jones, M.W., Andrew, R.M., Bakker, D.C., Hauck, J., Landschützer, P., Le Quéré, C.,
750 Luijkh, I.T., Peters, G.P., and Peters, W.: Global carbon budget 2023, *Earth Syst. Sci. Data*, 15(12), 5301-5369,
751 <https://doi.org/10.5194/essd-15-5301-2023>, 2023.

752

753 Fu, W., Randerson, J.T., and Moore, J.K.: Climate change impacts on net primary production (NPP) and export
754 production (EP) regulated by increasing stratification and phytoplankton community structure in the CMIP5 models,
755 *Biogeosciences*, 13(18), 5151-5170, <https://doi.org/10.5194/bg-13-5151-2016>, 2016.

756

757 Good, S., Fiedler, E., Mao, C., Martin, M.J., Maycock, A., Reid, R., Roberts-Jones, J., Searle, T., Waters, J., While, J.,
758 and Worsfold, M.: The current configuration of the OSTIA system for operational production of foundation sea surface
759 temperature and ice concentration analyses, *Remote Sens.*, 12(4), 720, <http://doi.org/10.3390/rs12040720>, 2020.

760

761 Hauck, J., Völker, C., Wang, T., Hoppema, M., Losch, M., and Wolf-Gladrow, D.A.: Seasonally different carbon flux
762 changes in the Southern Ocean in response to the southern annular mode, *Global Biogeochem. Cy.*, 27(4), 1236-1245,
763 <https://doi.org/10.1002/2013GB004600>, 2013.

764

765 Hawco, N.J., Tagliabue, A., and Twining, B.S.: Manganese limitation of phytoplankton physiology and productivity in
766 the Southern Ocean, *Global Biogeochem. Cy.*, 36(11), p.e2022GB007382, <https://doi.org/10.1029/2022GB007382>,
767 2022.

768

769 Henson, S.A., Sanders, R., Madsen, E., Morris, P.J., Le Moigne, F., and Quartly, G.D.: A reduced estimate of the
770 strength of the ocean's biological carbon pump, *Geophys. Res. Lett.*, 38(L04606), 1-5,
771 <https://doi.org/10.1029/2011GL046735>, 2011.

772

773 Henson, S.A., Sanders, R., and Madsen, E.: Global patterns in efficiency of particulate organic carbon export and
774 transfer to the deep ocean, *Global Biogeochem. Cy.*, 26(GB1028), 1-14, <http://dx.doi.org/10.1029/2011GB004099>,
775 2012.

776

777 Henson, S.A., Cael, B.B., Allen, S.R., and Dutkiewicz, S.: Future phytoplankton diversity in a changing climate, *Nat
778 Commun.*, 12, 5372, <https://doi.org/10.1038/s41467-021-25699-w>, 2021.

779

780 Henson, S.A., Laufkötter, C., Leung, S., Giering, S.L., Palevsky, H.I., and Cavan, E.L.: Uncertain response of ocean
781 biological carbon export in a changing world, *Nat. Geosci.*, 15(4), 248-254,
782 <https://doi.org/10.1038/s41561-022-00927-0>, 2022.

783

784 Jin, D., Hoagland, P., and Buesseler, K.O.: The value of scientific research on the ocean's biological carbon pump, *Sci.
785 Total Environ.*, 749, 141357, <https://doi.org/10.1016/j.scitotenv.2020.141357>, 2020.

786

787 Jönsson, B.F., Kulk, G., and Sathyendranath, S.: Review of algorithms estimating export production from satellite
788 derived properties, *Front.Mar. Sci.*, 10, 1149938, <https://doi.org/10.3389/fmars.2023.1149938>, 2023.

789

790 Kulk, G., Platt, T., Dingle, J., Jackson, T., Jönsson, B.F., Bouman, H.A., Babin, M., Brewin, R.J., Doblin, M., Estrada,
791 M., and Figueiras, F.G.: Primary production, an index of climate change in the ocean: satellite-based estimates over two
792 decades, *Remote Sens.*, 12(5), 826, <https://doi.org/10.3390/rs12050826>, 2020.

793

794 Kulk, G., Platt, T., Dingle, J., Jackson, T., Jönsson, B.F., Bouman, H.A., Babin, M., Brewin, R.J.W., Doblin, M., Estrada,
795 M., Figueiras, F.G., Furuya, K., González-Benítez, N., Gudfinnsson, H.G., Gudmundsson, K., Huang, B., Isada, T.,
796 Kovač, Ž., Lutz, V.A., Marañón, E., Raman, M., Richardson, K., Rozema, P.D., van de Poll, W.H., Segura, V., Tilstone,
797 G.H., Uitz, J., van Dongen-Vogels, V., Yoshikawa, T., and Sathyendranath, S.: BICEP / NCEO: Monthly global Marine
798 Phytoplankton Primary Production, between 1998-2020 at 9 km resolution (derived from the Ocean Colour Climate
799 Change Initiative v4.2 dataset), NERC EDS Centre for Environmental Data Analysis [data set],
800 <https://dx.doi.org/10.5285/69b2c9c6c4714517ba10dab3515e4ee6>, 2021.

801

802 Kwiatkowski, L., Aumont, O., Bopp, L., and Caias, P.: The impact of variable phytoplankton stoichiometry on
803 projections of primary production, food quality, and carbon uptake in the global ocean, *Global Biogeochem. Cy.*, 32(4),
804 516-528, <http://dx.doi.org/10.1002/2017GB005799>, 2018.

805

806 Kwiatkowski, L., Torres, O., Bopp, L., Aumont, O., Chamberlain, M., Christian, J.R., Dunne, J.P., Gehlen, M., Ilyina,
807 T., John, J.G., and Lenton, A.: Twenty-first century ocean warming, acidification, deoxygenation, and upper-ocean
808 nutrient and primary production decline from CMIP6 model projections, *Biogeosciences*, 17(13), 3439-3470,
809 <https://doi.org/10.5194/bg-17-3439-2020>, 2020.



810 Laufkötter, C., Vogt, M., and Gruber, N.: Long-term trends in ocean plankton production and particle export between
811 1960–2006, *Biogeosciences*, 10(11), 7373–7393, <https://doi.org/10.5194/bg-10-7373-2013>, 2013.

812
813 Laufkötter, C., Vogt, M., Gruber, N., Aita-Noguchi, M., Aumont, O., Bopp, L., Buitenhuis, E., Doney, S.C., Dunne, J.,
814 Hashioka, T., and Hauck, J.: Drivers and uncertainties of future global marine primary production in marine ecosystem
815 models, *Biogeosciences*, 12(23), 6955–6984, <https://doi.org/10.5194/bg-12-6955-2015>, 2015.

816
817 Laufkötter, C., Vogt, M., Gruber, N., Aumont, O., Bopp, L., Doney, S.C., Dunne, J.P., Hauck, J., John, J.G., Lima, I.D.,
818 and Seferian, R.: Projected decreases in future marine export production: the role of the carbon flux through the upper
819 ocean ecosystem, *Biogeosciences*, 13(13), 4023–4047, <https://doi.org/10.5194/bg-13-4023-2016>, 2016.

820
821 Laws, E.A., Falkowski, P.G., Smith Jr, W.O., Ducklow, H., and McCarthy, J.J.: Temperature effects on export
822 production in the open ocean, *Global Biogeochem. Cy.*, 14(4), 1231–1246, <https://doi.org/10.1029/1999GB001229>,
823 2000.

824
825 Laws, E.A., D'Sa, E., and Naik, P.: Simple equations to estimate ratios of new or export production to total production
826 from satellite-derived estimates of sea surface temperature and primary production, *Limnol. Oceanogr-Meth.*, 9(12),
827 593–601, <https://doi.org/10.4319/lom.2011.9.593>, 2011.

828
829 Li, Z., and Cassar, N.: Satellite estimates of net community production based on O₂/Ar observations and comparison to
830 other estimates, *Global Biogeochem. Cy.*, 30(5), 735–752, <https://doi.org/10.1002/2015GB005314>, 2016.

831
832 Longhurst, A., Sathyendranath, S., Platt, T., and Caverhill, C.: An estimate of global primary production in the ocean
833 from satellite radiometer data, *J. Plankton Res.*, 17(6), 1245–1271, <https://doi.org/10.1093/plankt/17.6.1245>, 1995.

834
835 Maier-Reimer, E., Mikolajewicz, U., and Winguth, A.: Future ocean uptake of CO₂: interaction between ocean
836 circulation and biology, *Clim. Dynam.*, 12, 711–722, <https://doi.org/10.1007/s003820050138>, 1996.

837
838 Monod, J.: The growth of bacterial cultures, *Annu. Rev. Microbiol.*, 3, 371–394,
839 doi:10.1146/annurev.mi.03.100149.002103, 1949.

840
841 Moore, J.K., Doney, S.C., Kleypas, J.A., Glover, D.M., and Fung, I.Y.: An intermediate complexity marine ecosystem
842 model for the global domain, *Deep-Sea Res. Pt. II*, 49(1–3), 403–462, [https://doi.org/10.1016/S0967-0645\(01\)00108-4](https://doi.org/10.1016/S0967-0645(01)00108-4),
843 2001.

844
845 Moore, J.K., Doney, S.C., and Lindsay, K.: Upper ocean ecosystem dynamics and iron cycling in a global
846 three-dimensional model, *Global Biogeochem. Cy.*, 18(GB4028), 1–21, <https://doi.org/10.1029/2004GB002220>, 2004.

847
848 Mouw, C.B., Barnett, A., McKinley, G.A., Gloege, L., and Pilcher, D.: Global ocean particulate organic carbon flux
849 merged with satellite parameters, *Earth Syst. Sci. Data*, 8(2), 531–541, <https://doi.org/10.5194/essd-8-531-2016>, 2004.

850
851 Nowicki, M., DeVries, T., and Siegel, D.A.: Quantifying the carbon export and sequestration pathways of the ocean's
852 biological carbon pump, *Global Biogeochem. Cy.*, 36(3), p.e2021GB007083, <https://doi.org/10.1029/2021GB007083>,
853 2022.

854
855 Palevsky, H.I., and Doney, S.C.: How choice of depth horizon influences the estimated spatial patterns and global
856 magnitude of ocean carbon export flux, *Geophys. Res. Lett.*, 45(9), 4171–4179,
857 <http://dx.doi.org/10.1029/2017GL076498>, 2018.

858
859 Richon, C., and Tagliabue, A.: Biogeochemical feedbacks associated with the response of micronutrient recycling by
860 zooplankton to climate change, *Glob. Change Biol.*, 27(19), 4758–4770, <https://doi.org/10.1111/gcb.15789>, 2021.

861
862 Ripple, W.J., Wolf, C., Gregg, J.W., Rockström, J., Mann, M.E., Oreskes, N., Lenton, T.M., Rahmstorf, S., Newsome,
863 T.M., Xu, C., and Svenning, J.C.: The 2024 state of the climate report: Perilous times on planet Earth, *BioScience*,
864 74(12), 812–824, <https://doi.org/10.1093/biosci/biae087>, 2024.

865
866 Ryan-Keogh, T.J., Thomalla, S.J., Chang, N., and Moalusi, T.: A new global oceanic multi-model net primary
867 productivity data product, *Earth Syst. Sci. Data*, 15(11), 4829–4848, <https://doi.org/10.5194/essd-15-4829-2023>, 2023.

868
869 Ryan-Keogh, T.J., Tagliabue, A., and Thomalla, S.J.: Global decline in net primary production underestimated by
870 climate models, *Commun. Earth Environ.*, 6(1), 75, <https://doi.org/10.1038/s43247-025-02051-4>, 2025.



871 Sabine, C.L., Feely, R.A., Gruber, N., Key, R.M., Lee, K., Bullister, J.L., Wanninkhof, R., Wong, C.S.L., Wallace, D.W.,
872 Tilbrook, B., and Millero, F.J.: The oceanic sink for anthropogenic CO₂, *Science*, 305(5682), 367-371,
873 <https://doi.org/10.1126/science.1097403>, 2004.

874

875 Sathyendranath, S., Brewin, R.J., Brockmann, C., Brotas, V., Calton, B., Chuprin, A., Cipollini, P., Couto, A.B., Dingle,
876 J., Doerffer, R., and Donlon, C.: An ocean-colour time series for use in climate studies: the experience of the
877 ocean-colour climate change initiative (OC-CCI), *Sensors*, 19(19), 4285, <https://doi.org/10.3390/s19194285>, 2019.

878

879 Séferian, R., Berthet, S., Yool, A., Palmiéri, J., Bopp, L., Tagliabue, A., Kwiatkowski, L., Aumont, O., Christian, J.,
880 Dunne, J., and Gehlen, M.: Tracking improvement in simulated marine biogeochemistry between CMIP5 and CMIP6,
881 *Curr. Clim. Change Rep.*, 6(3), 95-119, <https://doi.org/10.1007/s40641-020-00160-0>, 2020.

882

883 Siegel, D.A., Buesseler, K.O., Doney, S.C., Sailley, S.F., Behrenfeld, M.J., and Boyd, P.W.: Global assessment of ocean
884 carbon export by combining satellite observations and food-web models, *Global Biogeochem. Cy.*, 28(3), 181-196,
885 <https://doi.org/10.1002/2013GB004743>, 2014.

886

887 Sigman, D.M., and Boyle, E.A.: Glacial/interglacial variations in atmospheric carbon dioxide, *Nature*, 407(6806),
888 859-869, <https://doi.org/10.1038/35038000>, 2000.

889

890 Silsbe, G.M., Behrenfeld, M.J., Halsey, K.H., Milligan, A.J., and Westberry, T.K.: The CAFE model: A net production
891 model for global ocean phytoplankton, *Global Biogeochem. Cy.*, 30(12), 1756-1777,
892 <https://doi.org/10.1002/2016GB005521>, 2016.

893

894 Steinacher, M., Joos, F., Frölicher, T.L., Bopp, L., Cadule, P., Cocco, V., Doney, S.C., Gehlen, M., Lindsay, K., Moore,
895 J.K., and Schneider, B.: Projected 21st century decrease in marine productivity: a multi-model analysis, *Biogeosciences*,
896 7(3), 979-1005, <https://doi.org/10.5194/bg-7-979-2010>, 2010.

897

898 Tagliabue, A., Aumont, O., DeAth, R., Dunne, J.P., Dutkiewicz, S., Galbraith, E., Misumi, K., Moore, J.K., Ridgwell,
899 A., Sherman, E., and Stock, C.: How well do global ocean biogeochemistry models simulate dissolved iron
900 distributions?, *Global Biogeochem. Cy.*, 30(2), 149-174, <https://doi.org/10.1002/2015GB005289>, 2016.

901

902 Tagliabue, A., Bowie, A.R., Boyd, P.W., Buck, K.N., Johnson, K.S., and Saito, M.A.: The integral role of iron in ocean
903 biogeochemistry, *Nature*, 543(7643), 51-59, <https://doi.org/10.1038/nature21058>, 2017.

904

905 Tagliabue, A., Barrier, N., Du Pontavice, H., Kwiatkowski, L., Aumont, O., Bopp, L., Cheung, W.W., Gascuel, D., and
906 Maury, O.: An iron cycle cascade governs the response of equatorial Pacific ecosystems to climate change, *Glob.
907 Change Biol.*, 26(11), 6168-6179, <https://doi.org/10.1111/gcb.15316>, 2020.

908

909 Tagliabue, A., Kwiatkowski, L., Bopp, L., Butenschön, M., Cheung, W., Lengaigne, M., and Vialard, J.: Persistent
910 uncertainties in ocean net primary production climate change projections at regional scales raise challenges for assessing
911 impacts on ecosystem services, *Front. Clim.*, 3, 738224, <https://doi.org/10.3389/fclim.2021.738224>, 2021.

912

913 Tjiputra, J.F., Couespel, D., and Sanders, R.: Marine ecosystem role in setting up preindustrial and future climate, *Nat.
914 Commun.*, 16(1), 2206, <https://doi.org/10.1038/s41467-025-57371-y>, 2025.

915

916 Tréguer, P., Bowler, C., Moriceau, B., Dutkiewicz, S., Gehlen, M., Aumont, O., Bittner, L., Dugdale, R., Finkel, Z.,
917 Iudicone, D., and Jahn, O.: Influence of diatom diversity on the ocean biological carbon pump, *Nat. Geosci.*, 11(1),
918 27-37, <https://doi.org/10.1038/s41561-017-0028-x>, 2018.

919

920 Vichi, M., Pinardi, N., and Masina, S.: A generalized model of pelagic biogeochemistry for the global ocean ecosystem.
921 Part I: Theory, *J. Marine Syst.*, 64(1-4), 89-109, <https://doi.org/10.1016/j.jmarsys.2006.03.006>, 2007.

922

923 Visser, A.W.: Sequestration by the biological carbon pump: Do we really know what we are talking about?, *Limnol.
924 Oceanogr. Lett.*, 10(6), 851-858, <https://doi.org/10.1002/lo2.70053>, 2025.

925

926 Westberry, T., Behrenfeld, M.J., Siegel, D.A., and Boss, E.: Carbon-based primary productivity modeling with vertically
927 resolved photoacclimation, *Global Biogeochem. Cy.*, 22(2), 1-18, <https://doi.org/10.1029/2007GB003078>, 2008.

928

929 Westberry, T.K., Silsbe, G.M., and Behrenfeld, M.J.: Gross and net primary production in the global ocean: An ocean
930 color remote sensing perspective, *Earth-Sci Rev*, 237, 104322, <https://doi.org/10.1016/j.earscirev.2023.104322>, 2023.

931



932 Wilson, J.D., Andrews, O., Katavouta, A., de Melo Viríssimo, F., Death, R.M., Adloff, M., Baker, C.A., Blackledge, B.,
933 Goldsworth, F.W., Kennedy-Asser, A.T., and Liu, Q.: The biological carbon pump in CMIP6 models: 21st century
934 trends and uncertainties, *P. Natl. A. Sci.*, 119(29), p.e2204369119, <https://doi.org/10.1073/pnas.2204369119>, 2022.

935

936 World Meteorological Organization (WMO): <https://wmo.int/news/media-centre/>, last access: 21 January 2025.

937

938 Wrightson, L., and Tagliabue, A.: Quantifying the impact of climate change on marine diazotrophy: Insights from earth
939 system models, *Front. Mar. Sci.*, 7, 635, <https://doi.org/10.3389/fmars.2020.00635>, 2020.

940

941 Wrightson, L., Yang, N., Mahaffey, C., Hutchins, D.A., and Tagliabue, A.: Integrating the impact of global change on
942 the niche and physiology of marine nitrogen-fixing cyanobacteria, *Glob. Change Biol.*, 28(23), 7078-7093,
943 <https://doi.org/10.1111/gcb.16399>, 2022.

944

945 Wu, M., McCain, J.S.P., Rowland, E., Middag, R., Sandgren, M., Allen, A.E., and Bertrand, E.M.: Manganese and iron
946 deficiency in Southern Ocean *Phaeocystis antarctica* populations revealed through taxon-specific protein indicators, *Nat.*
947 *Commun.*, 10(1), 3582, <https://doi.org/10.1038/s41467-019-11426-z>, 2019.